ARTICLE

doi:10.1016/j.ymthe.2006.04.010

RNA Interference *in Vitro* and *in Vivo* Using a Chitosan/siRNA Nanoparticle System

Kenneth A. Howard,[1,2,*] Ulrik L. Rahbek,[1,2] Xiudong Liu,[1,2] Christian K. Damgaard,[1,2] Sys Zoffmann Glud,[1,2] Morten Ø. Andersen,[1,2] Mads B. Hovgaard,[1] Alexander Schmitz,[2] Jens R. Nyengaard,[3] Flemming Besenbacher,[1] and Jørgen Kjems[1,2]

[1]*Interdisciplinary Nanoscience Center (iNANO),* [2]*Department of Molecular Biology, and* [3]*Stereology and Electron Microscopy Research Laboratory, University of Aarhus, 8000 Aarhus C, Denmark*

**To whom correspondence and reprint requests should be addressed. Fax: (+45) 8942 3690. E-mail: kenh@inano.dk.*

Available online 10 July 2006

This work introduces a novel chitosan-based siRNA nanoparticle delivery system for RNA interference *in vitro* and *in vivo*. The formation of interpolyelectrolyte complexes between siRNA duplexes (21-mers) and chitosan polymer into nanoparticles, ranging from 40 to 600 nm, was shown using atomic force microscopy and photon correlation spectroscopy. Rapid uptake (1 h) of Cy5-labeled nanoparticles into NIH 3T3 cells, followed by accumulation over a 24 h period, was visualized using fluorescence microscopy. Nanoparticle-mediated knockdown of endogenous enhanced green fluorescent protein (EGFP) was demonstrated in both H1299 human lung carcinoma cells and murine peritoneal macrophages (77.9% and 89.3% reduction in EGFP fluorescence, respectively). In addition, Western analysis showed ~90% reduced expression of BCR/ABL-1 leukemia fusion protein while BCR expression was unaffected in K562 (Ph^+) cells after transfection using nanoparticles containing siRNA specific to the BCR/ABL-1 junction sequence. Effective *in vivo* RNA interference was achieved in bronchiole epithelial cells of transgenic EGFP mice after nasal administration of chitosan/siRNA formulations (37% and 43% reduction compared to mismatch and untreated control, respectively). These findings highlight the potential application of this novel chitosan-based system in RNA-mediated therapy of systemic and mucosal disease.

Key Words: RNA interference, siRNA, nanoparticles, chitosan, *in vivo*, nasal, pulmonary, BCR/ABL-1 protein, formactive

INTRODUCTION

RNA-mediated knockdown of protein expression at the messenger RNA (mRNA) level offers a new therapeutic strategy to overcome disease. The process by which small interfering RNA (siRNA) modulates enzymatic-induced cleavage of homologous mRNA and concomitant interruption of gene expression (RNA interference) has been extensively studied as a tool for investigating cellular processes in mammalian cells [1,2]. RNA interference has been demonstrated using siRNA directed against genes responsible for viral pathogenesis, cancer, and inflammatory conditions [3–5]. As a consequence, the possibility of silencing genes implicated in disease using siRNA has led to a rapidly evolving area in drug discovery.

The effectiveness of a drug is determined by the ability to migrate through the body and reach target sites at therapeutically relevant levels. Direct injection of naked siRNA using the hydrodynamic technique into the tail veins of mice has resulted in localized gene knockdown [6–10]. A drawback, however, is the requirement for high doses due to RNA instability and nonspecific cellular uptake and impracticality of this method for human use. Viral and non-viral delivery systems have been developed to overcome extracellular and intracellular barriers that restrict therapeutic use of nucleic acid-based drugs. Polyelectrolyte nanoparticles formed by self-assembly of plasmid DNA with polycations, widely used in gene delivery, have been adopted for siRNA use [11,12]. Cationic polymer and lipid-based siRNA vectors have been shown to enter cells and mediate specific RNA interference *in vitro* [13] and *in vivo* [4,14–16]. The effectiveness of nanoparticle systems is limited by rapid clearance from the circulation either by mononuclear phagocytic cell capture or non-specific cationic interactions with biological membranes and connective tissue [17]. An alternative approach for both local and systemic drug delivery is exploitation of mucosal routes, e.g., nasal, to avoid the first-pass hepatic clearance mechanism associated with intravenous administration. The polysaccharide chitosan,

1525-0016/$30.00

successfully used for nasal drug delivery due to mucoadhesive and mucosa permeation properties [18], has been utilized in the formation of polyelectrolyte nanoparticles containing plasmids for gene expression in respiratory sites and systemic tissue [19,20].

This work presents a novel chitosan/siRNA nanoparticle delivery system for *in vitro* and *in vivo* RNA interference applications. The concept is based on the use of an active siRNA agent (termed formactive component) to form nanoparticles through electrostatic bridges between chitosan polymeric chains. A detailed description of formulation and physicochemical characteristics significant to *in vivo* use such as size and morphology is followed by evaluation of nanoparticle uptake and RNA interference in a human carcinoma cell line and murine peritoneal macrophages expressing endogenous enhanced green fluorescent protein (EGFP). In addition, the ability of the system to mediate knockdown of the disease-associated BCR/ABL-1 protein is studied. To evaluate the potential use of this chitosan-based system for mucosal RNA interference applications, we investigated knockdown in a transgenic EGFP mouse model using the nasal route of administration.

RESULTS

Physicochemical Characterization

We determined physical properties such as size and surface charge that influence cellular interactions and nanoparticle biodistribution. All chitosan/siRNA formulations had a hydrodynamic radius lower than 350 nm by photon correlation spectroscopy (PCS) analysis (Table 1). The size of nanoparticle formation was dependent on the N:P ratio (defined as the ratio of chitosan amino groups (N) to RNA phosphate groups (P)) with increase in size at lower N:P. At low chitosan concentrations (250 μg/ml), nanoparticles formed at N:P 71 (formulation A) measured 181.6 nm but increased to 223.6 nm at N:P 6 (formulation B). Similarly, at high chitosan concentrations (1 mg/ml) the nanoparticle hydrodynamic radius increased from 139 nm at N:P 285 (formulation C) to 328 nm at N:P 23 (formulation D). This suggests more siRNA bond-forming bridges between chitosan chains at increased siRNA levels, leading to greater chitosan incorporation and possible interparticle aggregation. The observation that the saturation level of chitosan was reached in all formulations (verified by chitosan detection in particle filtrate, data not shown) confirms siRNA as the nanoparticle size determinant. The addition of salt over 24 h had no substantial effect on the hydrodynamic radius of the formulations studied. This may be due to repulsive forces between the particles being significantly stronger than hydrophobic self-association following neutralization of charge. ζ potential measurements showed that all formulations had a net positive charge greater than 18 mV (A, 26.8; B, 18.8; C, 29.5; and D, 31.1), reflecting excess chitosan at N:P greater than 1 (confirmed by acid urea gel analysis of chitosan, data not shown). The ζ potential decrease (18.8 mV) in B formed at lower levels of chitosan (250 μg/ml) and high siRNA reflects a greater chitosan incorporation and reduction in free material. Atomic force microscopy revealed a polydispersed distribution of predominantly spherical nanoparticles (Fig. 1). A population of extremely small discrete complexes (54–78 nm) was apparent in all the formulations (Figs. 1A–1D). We also observed large structures greater than 250 nm (size dependent on chitosan and siRNA concentration), suggesting recruitment of the smaller structures into aggregates (Figs. 1A–1D, insets). Complexes of 600 nm average length were formed with the highest chitosan and siRNA concentrations (Fig. 1D, inset).

We used the electrophoretic migration of siRNA to investigate complex formation and nanoparticle stability (Supplementary Fig. 1). Retardation of RNA within the gel showed complex formation between chitosan and siRNA at N:P 71 and 6. Interestingly, we observed slower migration at higher N:P ratio, suggesting the influence of increased amounts of free excess chitosan on particle stability. The requirement of polyanionic displacement with poly(L-aspartic) acid (PAA) for RNA release from the nanoparticles confirmed electrostatic chitosan/siRNA interactions. Moreover, intact siRNA was maintained after release from serum-incubated nanoparticles (N:P 71 and 6), whereas nonformulated naked RNA was degraded. This suggests that the chitosan effectively protects the siRNA against nuclease breakdown.

TABLE 1: Photon correlation spectroscopy of chitosan/siRNA nanoparticles

	Size (nm)/(polydispersity index)				
		Presence of salt[a]			
Formulation	Absence of salt	10 min	1 h	24 h	ζ potential (mV)
A (N:P 71)	181.6 (0.22)	173.2 (0.23)	175.9 (0.23)	176.4 (0.22)	26.8 (1.06)
B (N:P 6)	223.6 (0.19)	219.7 (0.21)	232.3 (0.23)	228.1 (0.20)	18.8 (2.11)
C (N:P 285)	139.0 (0.48)	132.8 (0.49)	138.0 (0.52)	136.3 (0.51)	29.5 (0.50)
D (N:P 23)	328.0 (0.24)	310.0 (0.23)	314.2 (0.24)	319.4 (0.23)	31.1 (0.74)

A and B, 250 μg/ml chitosan (M_r 114 kDa), and C and D, 1 mg/ml chitosan (M_r 114 kDa). Size and ζ potential average of three determinations, ζ potential SD in brackets.
[a] Incubation in 0.15 M NaCl before readings taken.

doi:10.1016/j.ymthe.2006.04.010

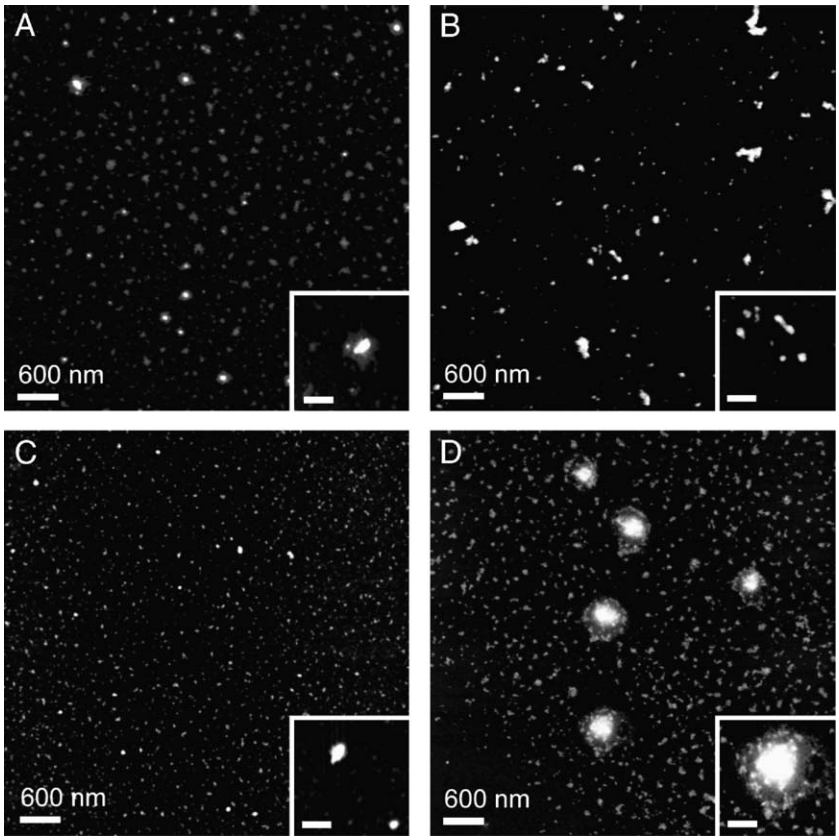

FIG. 1. Influence of chitosan and siRNA concentration on the formation of chitosan/siRNA nanoparticles. Atomic force microscopy images of chitosan/siRNA nanoparticles formed using 250 μg/ml chitosan, (A) N:P 71 and (B) N:P 6, and 1 mg/ml chitosan, (C) N:P 285 and (D) N:P 23. Insets show representative of large particles within image. (Large image 6 × 6 μm, scale bar, 600 nm; inset 1 × 1 μm, scale bar, 250 nm).

Cellular Studies

We investigated intracellular trafficking of nanoparticles containing Cy5-labeled siRNA (N:P 36) in live NIH 3T3 cells using semiconfocal epifluorescence microscopy (Fig. 2). Punctate fluorescence within the apical regions of cells, defining cellular borders, was visible after 1 h (Fig. 2A). At 4 h, fluorescence could be seen within all areas of the cytoplasm (Fig. 2B). The fluorescence was more diffuse in appearance compared to images taken at 1 h, suggesting possible particle dissociation and siRNA release. We found fluorescence throughout the cellular cytoplasm after 24 h (Fig. 2C).

We evaluated cellular cytotoxicity of chitosan and *Trans*IT-TKO-formulated particles in NIH 3T3 cells using a tetrazolium-based viability assay (Supplementary Fig. 2). Chitosan nanoparticles formed at N:P 71 (formulation A) and 285 (formulation C) reduced cell viability (31.5% and 39.8%, respectively) when added at a concentration of 50 nM siRNA/well. In contrast, and in accordance with *Trans*IT-TKO-treated cells, cell viability was maintained with chitosan nanoparticles formulated at low N:P (6 and 23, formulations B and D, respectively) using the same siRNA concentration. This suggests that excess chitosan in nanoparticles formed at high N:P may decrease cell viability related to the possible toxicity associated with high-molecular weight chitosan that has been reported previously [21]. This data provided information and guidelines for the development of noncytotoxic formulations (below N:P 71) taken forward into later transfection studies (refer to Fig. 3B).

We investigated RNA interference of endogenous protein expression in the H1299 cell line containing a stably integrated EGFP expression cassette and in primary macrophages from an EGFP transgenic mouse using nanoparticles containing EGFP-siRNA. We used the decrease in EGFP mean fluorescence intensity, detected by flow cytometry at 48 h post-transfection, as the measure of EGFP knockdown. Fig. 3A shows significant EGFP knockdown (77.9%) in H1299 cells 48 h post-transfection after an initial 4-h chitosan nanoparticle (N:P 57) transfection, levels comparable to those of *Trans*IT-TKO (78.0%). Knockdown was not significantly influenced in the presence of the endosomolytic agent chloroquine (66.4%), suggesting the capability of the nanoparticle system to escape endosomal compartments prior to RNA interaction with target mRNA. Chitosan nanoparticles containing EGFP-mismatch siRNA (4 bp mismatch) showed no EGFP knockdown, confirming knockdown specificity. Cellular viability in H1299 cells

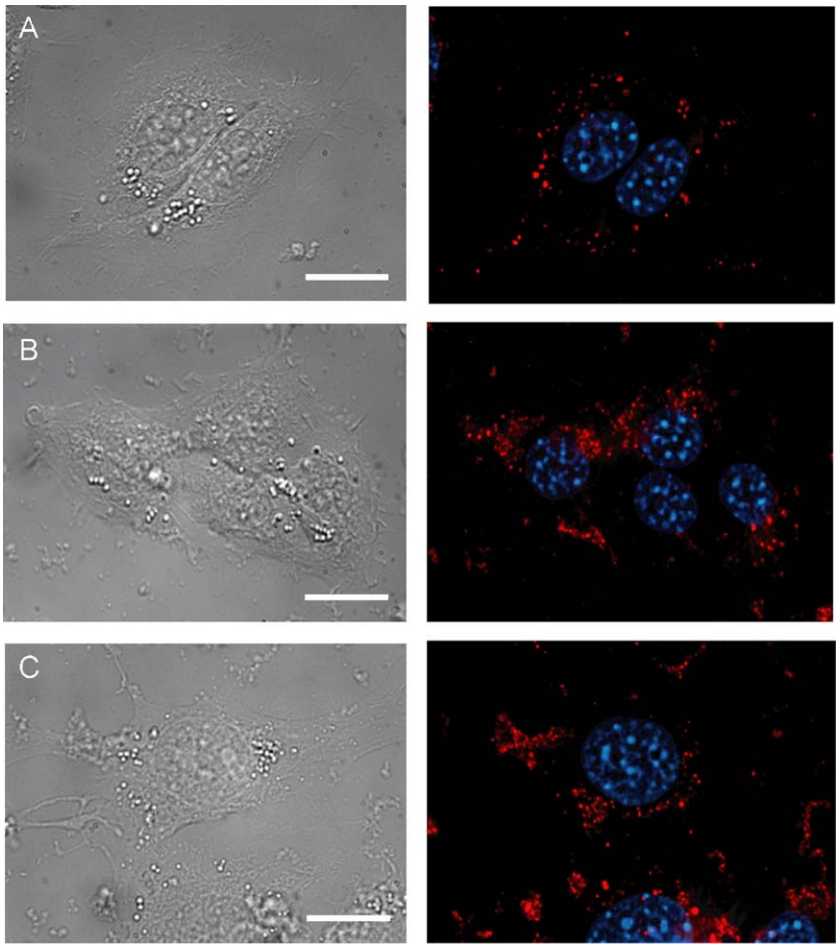

FIG. 2. Live cellular uptake of chitosan/siRNA nanoparticles into NIH 3T3 cells. Fluorescence microscopy was used to visualize cellular uptake and translocation of Cy5-labeled siRNA (100 nM/well) within chitosan nanoparticles (A, 1 h; B, 4 h; and C, 24 h). Images show fluorescent overlay of siRNA (red Cy5-labeled) and nuclei (blue Hoechst-labeled) adjacent to phase-contrast image (scale bar, 10 μm).

was maintained after addition of the different formulations used for transfection (Fig. 3B), dismissing the likelihood of toxicity effects.

The ability of the nanoparticle system (N:P 36) to mediate interference in primary cells was evaluated in peritoneal macrophages isolated from transgenic EGFP mice (Fig. 4). Macrophages, visualized by fluorescence microscopy, showed almost complete loss of EGFP fluorescence following 24 h post-transfection with chitosan nanoparticles (Figs. 4G and 4H) compared to untreated control (Figs. 4C and 4D), indicating significant knockdown. In contrast, cells transfected with *Trans*IT-TKO maintained EGFP expression (Figs. 4E and 4F). We verified this trend using flow cytometric measurements of samples (Fig. 4I). We found high levels of EGFP knockdown in cells treated with nanoparticles (86.9%) compared to *Trans*IT-TKO (no knockdown detected) (Fig. 4I). This correlates with the avid uptake into macrophages shown by nanoparticles containing Cy5-labeled siRNA (Figs. 4A and 4B). Increasing the siRNA concentration from 100 to 200 nM did not greatly increase knockdown levels in either nanoparticle (89.3% compared to 86.9%) or *Trans*IT-TKO transfections.

We tested the ability of the nanoparticles to knock down expression of the BCR/ABL-1 oncogene, found in chronic myelogenous leukemia, to demonstrate the therapeutic potential of the chitosan system (Supplementary Fig. 3). We transfected the BCR/ABL-1-expressing cell line K562 transiently with nanoparticles (N:P 57) complexed with either a fusion-specific or a non-specific siRNA. Western blotting analysis using an antibody recognizing the N-terminal part of BCR, demonstrated ~90% BCR/ABL-1 knockdown in cells transfected with nanoparticles containing BCR/ABL-1-specific siRNA.

Pulmonary RNA Interference

We used a transgenic EGFP mouse model [22] to investigate the ability of chitosan-based systems to mediate EGFP knockdown following nasal administration. None of the mice appeared to have any adverse effects from daily nasal administration of chitosan nanoparticles (N:P 6) over the 5-day period. We sub-

doi:10.1016/j.ymthe.2006.04.010

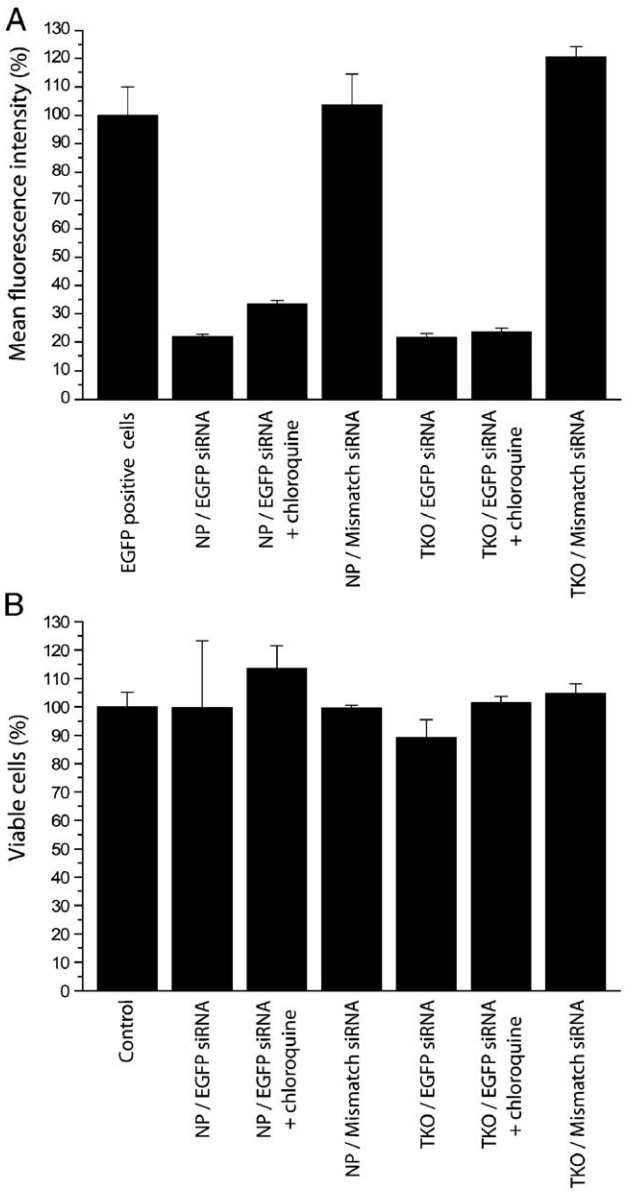

FIG. 3. Nanoparticle-mediated RNA interference in the EGFP-H1299 cell line. (A) EGFP-H1299 cell line transfection with chitosan/EGFP-specific siRNA nanoparticles (NP) or *Trans*IT/TKO/EGFP-specific siRNA for 4 h (50 nM siRNA/well) with or without chloroquine (10 μM/well). The decrease in EGFP mean fluorescence intensity, detected by flow cytometry at 48 h post-transfection, was used as the measure of EGFP knockdown (normalized to % control untreated EGFP cells, error bars represent ±SD). Chitosan/EGFP-mismatch siRNA NP or *Trans*IT/TKO/EGFP-mismatch siRNA controls are also shown. (B) EGFP-H1299 cell viability after treatment with same formulations used in transfection study (normalized to % control untreated cells) (error bars represent ±SD).

jected the mice to whole body perfusion fixation following siRNA treatment and investigated lung sections by fluorescence microscopy. In two separate experiments, mice dosed with nanoparticles containing EGFP siRNA clearly showed reduced numbers of EGFP-expressing epithelial cells in the bronchioles (43% compared to untreated mice control (experiment 1, Fig. 5C) and 37% compared to EGFP-mismatch control (experiment 2, Fig. 5D). Representative images of control (Fig. 5A) and knockdown (Fig. 5B) are shown. We observed this phenomenon both in lower and in upper regions of the lung. We calculated the number of green cells as a percentage of 200 cells per tissue section (experiment 1, Fig. 5C) or total numbers in the whole left lung (experiment 2, Fig. 5D) by stereological counting. The presence of DAPI-stained nuclei demonstrated an intact epithelial bronchiole border in control and nanoparticle-dosed mice following treatment and histological processing.

DISCUSSION

In this study, we introduce a novel chitosan-based siRNA delivery system for RNA interference protocols, the rationale based on the exploitation of chitosan properties to allow mucosal delivery. The focus of this work was directed toward development of systems capable of gene silencing at respiratory sites; therefore, the nasal route of administration was investigated using a transgenic EGFP mouse as a knockdown model.

Self-assembly of siRNA into nanoparticles was achieved at low (250 μg/ml) and high (1 mg/ml) chitosan concentrations with RNA sufficient in length (21 nucleotides) to meet the 6–10 salt bond requirement for the formation of a cooperative system between polyelectrolyte species [23]. Atomic force microscopy analysis revealed a predominate population of small discrete particles in the 50 nm size range and a larger subpopulation ranging from 200 to 500 nm, suggesting interparticle aggregation following initial entropy-driven particle formation. This was confirmed by PCS measurements, which showed small and large hydrodynamic radii distributed around a mean of 180–330 nm. In accordance with drug delivery requirements, release of structurally intact siRNA from the nanoparticles was demonstrated by electrophoresis, an essential prerequisite for nanocarrier-mediated RNA gene silencing.

As much as 77.9% specific reduction of EGFP fluorescence was measured in an EGFP-H1299 human lung carcinoma cell line transfected for 4 h with chitosan nanoparticles. These levels were similar to knockdown observed in cells transfected for the longer period of 24 h with *Trans*IT-TKO transfection reagent. The relatively short transfection time required when using chitosan is probably a result of the rapid siRNA accumulation observed in NIH 3T3 cells within a 4-h period using chitosan nanoparticles. The cellular uptake properties of chitosan nanoparticles can be attributed to the small particle size and excess positive charge that facilitate

interaction with cellular membranes. Transfection in the presence of the endosomolytic agent chloroquine did not increase RNA interference with the chitosan system, indicating an endosomal escape mechanism for the chitosan-based system. In support of this, a diffuse cellular distribution of Cy5-labeled siRNA was visualized throughout the whole cytoplasm with no evidence of compartmentalization in NIH 3T3 cells. The endosomolytic property of chitosan/DNA nanoparticles has been reported previously; being ascribed to a proton sponge mechanism [24] combined with endosomal membrane rupture as a consequence of polycation swelling under acidic conditions [25].

The therapeutic potential of chitosan nanoparticles for knockdown of disease-related proteins was demonstrated in K562 cells endogenously expressing BCR/ABL-1 protein. Transfection with a single treatment of chitosan nanoparticles containing breakpoint siRNA resulted in ~90% allele-specific knockdown. The chitosan system was the only chemical transfection agent, including commercial alternatives, that successfully showed BCR/ABL-1 knockdown in this suspension cell line in our experiments (data not shown). In comparison to other polycation-based polyethylenimine systems [11,16] that have reported knockdown in adherent cell lines, our work shows efficient knockdown in both adherent and suspension cells.

Macrophages are important cells in inflammatory and viral disease and consequently a target for RNA interference therapies. Retroviral vectors have been shown to mediate RNA interference in primary cells [26]; however, concerns remain over retrovirus inflammatory and safety issues. Recently, Song *et al.* [3] demonstrated a sustained siRNA effect in primary macrophages using cationic lipids, promoting the development of non-viral alternatives. In our experiments, peritoneal macrophages isolated from transgenic EGFP mice were used to evaluate chitosan-based knockdown in primary cells and to provide an appropriate pre-*in vivo* model. We showed 89.3% reduced EGFP levels (compared to untreated cells) within 1 day following a single 4-h treatment with chitosan nanoparticles, which correlates with rapid uptake of chitosan nanoparticles into these cells in less than 4 h. In contrast, *Trans*IT-TKO transfection gave no significant EGFP knockdown under the same conditions. To our knowledge, this is the first report showing knockdown in primary macrophages with a polycation-based system. Chitosan-mediated transfection in macrophages may be linked to the ability of chitosan to activate and enter macrophages via mannose-type lectin receptors [27,28] combined with the ability of macrophages to phagocytose nanoparticles of the described size range. An expected consequence for systemic delivery, however, is rapid clearance of the nanoparticle system from the circulation by cellular components of the mononuclear phagocyte system such as Kupffer cells found in the liver.

The nasal route offers a non-invasive alternative to the systemic administration of siRNA therapeutics. It provides direct access to respiratory tissue and a migration pathway to systemic sites with avoidance of first-pass hepatic clearance. Our strategy is to exploit the mucoadhesive and permeation properties of chitosan for effective delivery and RNA interference at respiratory sites, as an approach to treat pulmonary disease. The transgenic EGFP mouse used in our experiments showed significant EGFP knockdown (43% compared to untreated control and 37% compared to EGFP-mismatch) within bronchiole epithelial cells following a nasal dose of nanoparticles containing EGFP-specific siRNA. This is the first documentation to our knowledge of knockdown within this cell type after nasal administration. The role of chitosan is supported by a previous finding showing that chitosan/DNA particles adhere to bronchiole epithelia and facilitate gene expression in this region after intratracheal administration [19]. The use of a pulmonary active surface material (InfaSurf) for alveoli delivery and knockdown with GAPDH siRNA further supports the use of mucoadhesive compounds for lung transfection [29]. The application of a nebulization method has recently been shown to improve chitosan/DNA nanoparticle distribution and gene expression in mouse lung, emphasizing the importance of delivery techniques for particle localization [30]. Future work in our laboratory is directed toward the development of aerosol forms for our chitosan/siRNA system.

This work introduces a versatile siRNA nanocarrier that can be used for both *in vitro* and *in vivo* RNA interference protocols. We are currently working on second generation systems containing essential components built into the design and pulmonary delivery techniques to further maximize activity, essential requirements in order to realize the therapeutic potential of this system.

Materials and Methods

Chemicals and siRNA. Chitosan (114 kDa, 84% deacetylation) was produced by Bioneer A/S (Hørsholm, Denmark). EGFP-specific siRNA duplex purchased from Dharmacon containing the sequences sense, 5′-GACGUAAACGGCCACAAGUUC-3′, and antisense, 3′-CGCUGCAUUUGCCGGUGUUCA-5′, and EGFP-mismatch sense, 5′-GACGUUAGACUGACAAGUUC-3′, and antisense, 3′-CGCUGAAUCUGACCUGUGGUUCA-5′, were used for nanoparticle characterization studies and EGFP interference work. EGFP siRNA containing a fluorescent Cy5-labeled 5′ sense strand was used for cellular uptake studies. BCR/ABL-1 siRNA target sequence, AAGCAGAGUUCAAAAGCCCUU, and control target sequence, AAGGAGAAUAGCAGAAUGCAU, were used for leukemia translocation protein knockdown. The mouse hnRNP C1 antibody was a gift from Seraphin Pinol-Roma. *Trans*IT-TKO siRNA transfection agent was purchased from Mirus Corp. (USA). SYBR gold nucleic acid stain was purchased from Molecular Probes (Eugene, OR, USA) and PAA from Sigma–Aldrich (Poole, Dorset, UK).

Formation of chitosan/siRNA nanoparticles. Chitosan (114 kDa) was dissolved in sodium acetate buffer (0.2 M NaAc, pH 4.5) to obtain a 0.2–1 mg/ml working solution range. Twenty microliters of siRNA (20–250 μm range) was added to 1 ml of filtered chitosan while stirring and left for 1 h. To calculate specific N:P ratios (defined as the molar ratio of chitosan

doi:10.1016/j.ymthe.2006.04.010

amino groups/RNA phosphate groups) a mass per phosphate of 325 Da was used for RNA and mass per charge of 167.88 for chitosan (84% deacetylation).

Photon correlation spectroscopy and determination of surface charge on chitosan/siRNA nanoparticles. The hydrodynamic size of chitosan/siRNA complexes was determined by PCS using a Zetasizer Nano ZS (Malvern Instruments, Malvern, UK). PCS was performed at 25°C in sodium acetate buffer in triplicate with sampling time and analysis set to automatic. Particle size is presented as the *z* average of three measurements ± SD. To investigate the effect of salt on hydrodynamic size, sodium chloride (final concentration 150 mM) was added to the particle solution for set time points before remeasurement. Surface charge was measured by determination of ζ potential using a Zetasizer Nano ZS in sodium acetate buffer.

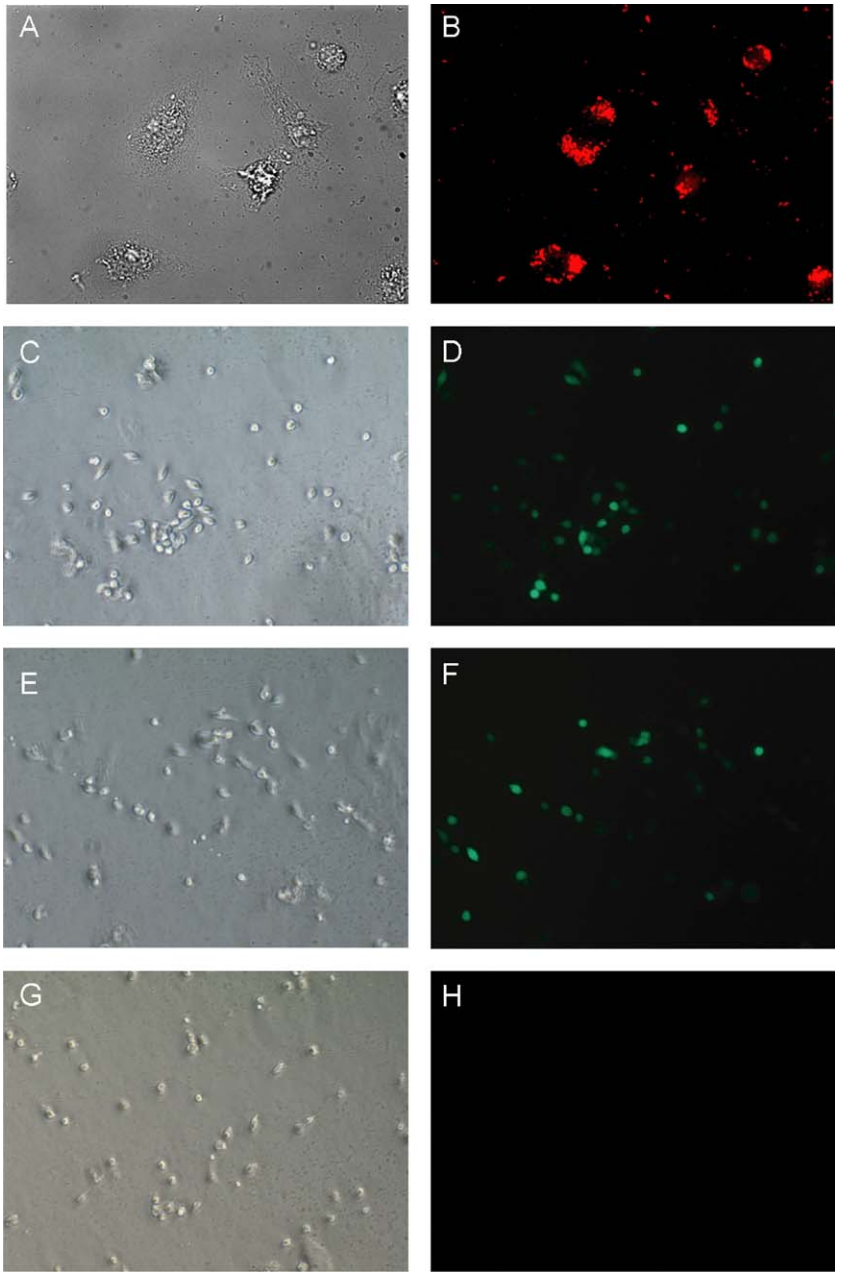

FIG. 4. Nanoparticle-mediated RNA interference in primary macrophages. EGFP knockdown in macrophages isolated from EGFP transgenic mice is shown. Fluorescence micrographs showing chitosan nanoparticle uptake after 4 h (A, light image; B, Cy5-labeled siRNA (red)). Untreated EGFP macrophages (C, light image; D, cellular EGFP fluorescence (green), macrophage cellular fluorescence 24 h post-transfection with EGFP-specific siRNA (100 nM/well for 4 h) with *Trans*IT-TKO (E and F), and chitosan nanoparticles (ND) (G and H). (I) Flow cytometric analysis of macrophage EGFP fluorescence. In addition, analysis of cells transfected with 200 nM siRNA is presented. Peritoneal primary macrophages isolated from nongreen mice were used as an EGFP-negative control.

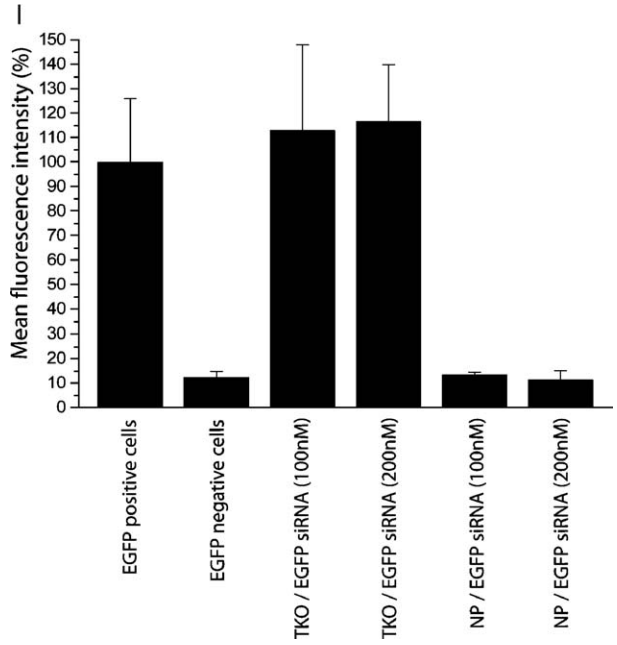

FIG. 4 (*continued*).

Determination of nanoparticle morphology using atomic force microscopy. Chitosan/siRNA nanoparticles were diluted 1/10 using 0.2-μm filtered sodium acetate buffer. A sample volume of 15 μl was immobilized onto freshly cleaved mica. The samples were purged with N_2 and imaged in Tapping Mode under ambient conditions on a nanoscope IIIA (Digital Instruments) using NSG01 (NT-MDT) cantilevers with a tip radius less than 10 nm. Several images were obtained for each sample, ensuring data reproducibility.

Cellular uptake of Cy5-labeled siRNA chitosan nanoparticles. NIH 3T3 cells or mouse peritoneal macrophages were cultured in 35-mm dishes with glass coverslip bottoms and transfected with 100 nM Cy5-labeled sense-strand EGFP siRNA using chitosan nanoparticles (N:P 36). The cells were transfected with the nanoparticles in serum-free DMEM for 1–4 h after which 10% serum was added. Following transfection cells were subjected to Hoechst staining to visualize nuclei. Uptake of duplex siRNA was monitored by a Zeiss semiconfocal epifluorescence microscope.

RNA interference in EGFP-expressing human cell line and primary murine macrophages. The human lung cancer cell line H1299 produced to express EGFP stably (EGFP half-life 2 h) was a gift from Dr. Anne Chauchereau (CNRS, Villejuif, France). Cells were plated on multiwell 24-well plates (10^5 cells/well) in RPMI media (containing 10% fetal bovine serum (FBS), 5% penicillin/streptomycin, and 418 selection factor) 24 h prior to transfection. The medium was removed and replaced with 250 μl fresh medium (with or without FBS). The cells were transfected with chitosan/siRNA nanoparticles or *Trans*IT-TKO transfection reagent at 50 nM siRNA (EGFP-specific or EGFP-mismatch) per well in the presence or absence of chloroquine (10 μM per well, added 10 min prior to addition of siRNA). After 4 h, the medium was replaced with 0.5-ml fresh medium containing 10% FBS. The cells were left for 48 h and then removed using a standard trypsin protocol and resuspended in PBS containing 1% paraformaldehyde. The EGFP cell fluorescence was measured using a Becton–Dickinson FACSCalibur flow cytometer. A histogram plot with log green fluorescence intensity on the *x* axis and cell number on the *y* axis was used to define median fluorescence intensity of the main cell population defined by scatter properties (forward and side scatter, not shown).

Adult EGFP-transgenic mice (C57BL/6-Yg (ACTbEGFP) 1Osb/J) (The Jackson Laboratory, Bar Harbor, ME, USA) were killed by cervical dislocation and injected intraperitoneally with 5 ml of MEM containing 20% FBS. The abdomen was agitated gently, the peritoneum exposed and breached, and the medium removed using a syringe. The medium was centrifuged (2500 rpm for 10 min) and the pellet resuspended in MEM containing 50% FBS. The suspension was plated on a multiwell 12-well plate. The macrophages were allowed to adhere for 2 h before medium (containing nonadherent cells) was removed. Fresh medium containing 5% penicillin/streptomycin was then added to the cells. After 40 h the medium was removed and replaced with MEM without FBS and chitosan/siRNA nanoparticles or *Trans*IT-TKO/siRNA added. After 4 h, medium was

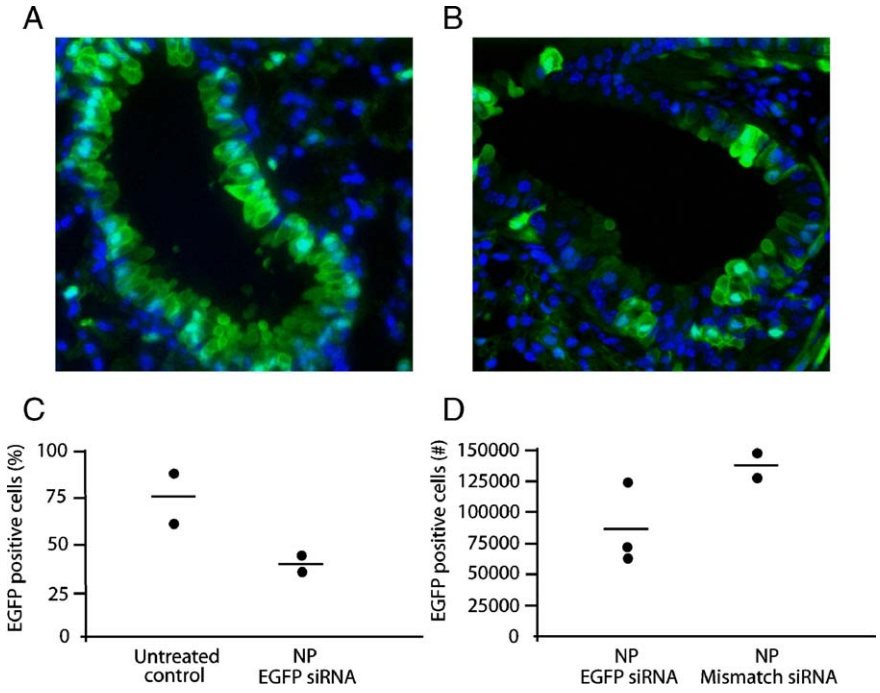

FIG. 5. Pulmonary RNA interference in the transgenic EGFP mouse. The number of EGFP-expressing endothelial cells of the bronchioles was counted by fluorescence microscopy in 3-μm lung sections taken from EGFP mice (n = 2 or 3) nasally dosed with chitosan/EGFP-siRNA nanoparticles (30 μg siRNA per day for 5 days) (two separate experiments presented). The representative images show EGFP fluorescence (green) and DAPI-stained nuclei (blue) overlays within the bronchiole region of (A) control mice and (B) mice treated with chitosan/EGFP-specific siRNA nanoparticles. The numbers of EGFP-positive cells expressed as a percentage (%) of 200 epithelial cells counted are presented in C (experiment 1, untreated mice used as control) and total numbers of EGFP-positive cells (#) from whole left lung are presented in D (experiment 2, EGFP-mismatch used as control).

doi:10.1016/j.ymthe.2006.04.010

removed and replaced with fresh medium containing 10% FBS. After 24 h the cells were processed and analyzed for EGFP fluorescence using a BD FACSCalibur flow cytometer or visualized using a Zeiss semiconfocal epifluorescence microscope. Untreated macrophages isolated from C57BL/6J mice were used as non-fluorescent controls.

Pulmonary RNA interference in EGFP mouse. EGFP-transgenic mice (C57BL/6-Yg(ACTbEGFP)1Osb/J) used for *in vivo* siRNA studies were housed in SFP conditions under strict veterinary supervision at Pipeline Biotech A/S (Trige, Denmark). Chitosan/siRNA particles were concentrated to 1 mg/ml siRNA using VivaSpin20 centrifugal concentrators (MW cut-off 100 kDa; Vivascience) prior to dosing. In two different experiments, a total of 30 μl of particles was administered intranasally (15 μl per nostril) each day over 5 consecutive days to the EGFP mice (nondosed C57BL/6J mice were used as control in experiment 1 and EGFP-mismatch as control in experiment 2). At day 6 mice were anesthetized with an injection of 0.14 ml zoletilmix/torbugesic mix and perfusion fixated manually with 4% formaldehyde phosphate-buffered solution (Volusol; VWR International). Lungs were harvested, paraffin embedded, and cut exhaustively in 3-μm sections and every 100th section together with the next was sampled. Sections were transferred into DAPI (Sigma, St. Louis, MO, USA) solution for counterstaining and wet mounted on a Super Frost slide. Slides were analyzed in a fluorescence microscope (Olympus BX 51; Tokyo, Japan) with a UV/GFP filter, a 20× objective, a mounted digital camera (Olympus DP-70), and a motorized stage in conjunction with CAST software (Visiopharm, Copenhagen, Denmark). The number of EGFP-expressing epithelial bronchial cells was counted by a physical fractionator.

ACKNOWLEDGMENTS

The authors thank Mads Johnsen (Bioneer A/S) for providing chitosan samples and Anne Chauchereau for providing the EGFP-expressing H1299 cell line used in this work. We are also grateful to Tonnie Holm Nygaard for excellent technical assistance and Annette Sorensen for supervision of animal experiments conducted at Pipeline A/S. The authors acknowledge Martin Read and Karina Dalsgaard Sørensen for constructive comments. The work was supported by the Danish Technical Research Council, the Danish Strategic Research Council, the Danish Cancer Society, and the EU-FP6 RIGHT program.

RECEIVED FOR PUBLICATION NOVEMBER 18, 2005; REVISED MARCH 31, 2006; ACCEPTED APRIL 10, 2006.

APPENDIX A. SUPPLEMENTARY DATA

Supplementary data associated with this article can be found, in the online version, at doi:10.1016/j.ymthe.2006.04.010.

REFERENCES

1. Lieberman, J., Song, E., Lee, S. K., and Shankar, P. (2003). Interfering with disease: opportunities and roadblocks to harnessing RNA interference. *Trends Mol. Med.* **9:** 397–403.
2. Tuschl, T. (2001). RNA interference and small interfering RNAs. *Chembiochemistry* **2:** 239–245.
3. Song, E., *et al.* (2003). Sustained small interfering RNA-mediated human immunodeficiency virus type 1 inhibition in primary macrophages. *J. Virol.* **77:** 7174–7181.
4. Yano, J., *et al.* (2004). Antitumor activity of small interfering RNA/cationic liposome complex in mouse models of cancer. *Clin. Cancer Res.* **10:** 7721–7726.
5. Flynn, M. A., Casey, D. G., Todryk, S. M., and Mahon, B. P. (2004). Efficient delivery of small interfering RNA for inhibition of IL-12p40 expression in vivo. *J. Inflammation (London)* **1:** 4.
6. Lewis, D. L., *et al.* (2002). Efficient delivery of siRNA for inhibition of gene expression in postnatal mice. *Nat. Genet.* **32:** 107–108.
7. Mccaffrey, A. P., *et al.* (2002). RNA interference in adult mice. *Nature* **418:** 38–39.
8. Kobayashi, N., *et al.* (2004). Vector-based in vivo RNA interference: dose- and time-dependent suppression of transgene expression. *J. Pharmacol. Exp. Ther.* **308:** 688–693.
9. Layzer, J. M., *et al.* (2004). In vivo activity of nuclease-resistant siRNAs. *RNA* **10:** 766–771.
10. Lewis, D. L., and Wolff, J. A. (2005). Delivery of siRNA and siRNA expression constructs to adult mammals by hydrodynamic intravascular injection. *Methods Enzymol.* **392:** 336–350.
11. Schiffelers, R. M., *et al.* (2004). Cancer siRNA therapy by tumor selective delivery with ligand-targeted sterically stabilized nanoparticle. *Nucleic Acids Res.* **32:** e149.
12. Thomas, M., *et al.* (2005). Full deacylation of polyethylenimine dramatically boosts its gene delivery efficiency and specificity to mouse lung. *Proc. Natl. Acad. Sci. USA* **102:** 5679–5684.
13. Takahashi, Y., Nishikawa, M., Kobayashi, N., and Takakura, Y. (2005). Gene silencing in primary and metastatic tumors by small interfering RNA delivery in mice: quantitative analysis using melanoma cells expressing firefly and sea pansy luciferases. *J. Controlled Release* **105:** 332–343.
14. Sioud, M., and Sorensen, D. R. (2003). Cationic liposome-mediated delivery of siRNAs in adult mice. *Biochem. Biophys. Res. Commun.* **312:** 1220–1225.
15. Sorensen, D. R., Leirdal, M., and Sioud, M. (2003). Gene silencing by systemic delivery of synthetic siRNAs in adult mice. *J. Mol. Biol.* **327:** 761–766.
16. Urban-Klein, B., *et al.* (2005). RNAi-mediated gene-targeting through systemic application of polyethylenimine (PEI)-complexed siRNA in vivo. *Gene Ther.* **12:** 461–466.
17. Nishida, K., *et al.* (1991). Hepatic disposition characteristics of electrically charged macromolecules in rat in vivo and in the perfused liver. *Pharm. Res.* **8:** 437–444.
18. Illum, L. (2003). Nasal drug delivery—Possibilities, problems and solutions. *J. Controlled Release* **87:** 187–198.
19. Koping-Hoggard, M., *et al.* (2001). Chitosan as a nonviral gene delivery system: structure–property relationships and characteristics compared with polyethylenimine in vitro and after lung administration in vivo. *Gene Ther.* **8:** 1108–1121.
20. Iqbal, M., *et al.* (2003). Nasal delivery of chitosan–DNA plasmid expressing epitopes of respiratory syncytial virus (RSV) induces protective CTL responses in BALB/c mice. *Vaccine* **21:** 1478–1485.
21. Richardson, S. C., Kolbe, H. V., and Duncan, R. (1999). Potential of low molecular mass chitosan as a DNA delivery system: biocompatibility, body distribution and ability to complex and protect DNA. *Int. J. Pharm.* **178:** 231–243.
22. Okabe, M., *et al.* (1997). 'Green mice' as a source of ubiquitous green cells. *FEBS Lett.* **407:** 313–319.
23. Vinogradov, S. V., Bronich, T. K., and Kabanov, A. V. (1998). Self-assembly of polyamine–poly(ethylene glycol) copolymers with phosphorothioate oligonucleotides. *Bioconjugate Chem.* **9:** 805–812.
24. Huang, M., Fong, C. W., Khor, E., and Lim, L. Y. (2005). Transfection efficiency of chitosan vectors: effect of polymer molecular weight and degree of deacetylation. *J. Controlled Release* **106:** 391–406.
25. Ishii, T., Okahata, Y., and Sato, T. (2001). Mechanism of cell transfection with plasmid/chitosan complexes. *Biochim. Biophys. Acta* **1514:** 51–64.
26. Barton, G. M., and Medzhitov, R. (2002). Retroviral delivery of small interfering RNA into primary cells. *Proc. Natl. Acad. Sci. USA* **99:** 14943–14945.
27. Mori, T., *et al.* (2005). Mechanism of macrophage activation by chitin derivatives. *J. Vet. Med. Sci.* **67:** 51–56.
28. Feng, J., Zhao, L., and Yu, Q. (2004). Receptor-mediated stimulatory effect of oligochitosan in macrophages. *Biochem. Biophys. Res. Commun.* **317:** 414–420.
29. Massaro, D., Massaro, G. D., and Clerch, L. B. (2004). Noninvasive delivery of small inhibitory RNA and other reagents to pulmonary alveoli in mice. *Am. J. Physiol. Lung Cell Mol. Physiol.* **287:** L1066–L1070.
30. Koping-Hoggard, M., *et al.* (2005). A miniaturized nebulization catheter for improved gene delivery to the mouse lung. *J. Gene Med.* **7:** 1215–1222.